Dynamic Fracture Characterization of a Pressure Vessel Steel

W. SCHMITT, W. BÖHME, W. KLEMM, D. MEMHARD, S. WINKLER
Fraunhofer-Institut fur Werkstoffmechanik, Freiburg, FRG

1. INTRODUCTION

Dynamic events are characterized by time- and space-dependent stress and strain fields caused by wave or inertia effects. Dynamic effects at cracks may be originated from rapid loading rates or impact loading of a structure containing a stationary crack or by the time-dependent stress and strain field of a propagating or arresting crack itself. Dynamic effects complicate the analysis of the crack tip stress and strain fields and usually considerable experimental efforts and numerical techniques are required. Higher loading rates influence the material behaviour, not only with respect to deformation and yield behaviour but also with respect to fracture toughness.

In the context of reactor safety the behaviour of propagating and arresting cracks is important:

While for normal operation and emergency conditions the exclusion of crack initiation and extension is essential, for faulted conditions the regulations (e.g., the German KTA) may tolerate crack initiation provided that it can be shown that the crack will be arrested within 75% of the wall thickness. This leads to the problem of crack arrest in the upper shelf of the Charpy energy.

In order to evaluate accident sequences and possible consequences of pipe failures the propagation and arrest behaviour of cracks in pipes must be known. Due to the elevated temperatures the fracture mode would be ductile and methods of elastic-plastic fracture mechanics must be applied considering large amounts of crack extension and dynamic effects.

For this purpose a heat of a German reactor pressure vessel steel was investigated:

dynamic J-resistance curves were evaluated from impact-loaded large three-point-bend specimens,

the crack propagation energy at large amounts of crack extension was determined with wide tension plates.

2. DYNAMIC J-RESISTANCE CURVES

In order to quantify the toughness properties during fast crack propagation dynamic fracture resistance curves were measured. With impact velocities of several m/s loading rates were achieved which were five to six orders of magnitude above usual static loading rates and which may be considered as an upper limit to loading rates expected during postulated emergency and faulted conditions.

The investigations were carried out with the ferritic pressure vessel steel ASTM A 508 Cl 2 (22 NiMoCr 3 7) at temperatures in the upper shelf regime of the Charpy energy. The

examinations focused on details of the initiation process and the ductile crack extension [1-3].

2.1 Experiments

Large bend specimens (SENB) with dimensions 495 mm × 90 mm × 45 mm were fabricated, fatigued to initial crack lengths of a_o = 45,6 ± 1,4 mm, and side-grooved (20%). The specimens were loaded in three-point bending in a drop-weight tower (see Fig. 1) with an impact velocity of 6,77 m/s. Using different hammer masses between 111 kg and 282 kg the impact energy was varied and thus different amounts of ductile crack extension could be achieved in different tests.

From undeformed parts of broken specimens Charpy specimens with the standard dimensions were fabricated, provided with fatigue cracks (a_o = 5,5 ± 0,3 mm) and sidegrooves (20%), and loaded in a pendulum with a hammer mass of 20 kg. Different amounts of ductile crack extension were achieved by the variation of the impact velocity between 0,55 m/s and 1,73 m/s.

In all experiments the load P at the tup of the impacting hammer was measured by means of statically calibrated strain gauges and recorded as a function of the time t. The time-dependent displacement of the hammer, s(t), was calculated from P(t) by Newton's second law of motion. A characteristic example of the resulting load-displacement record P(s) for the SENB specimens is given in Fig. 2.

In the experiments with SENB specimens further measurements were made simultaneously. Almost all specimens were supplied with strain gauges near the crack tip in order to get some information about the actual loading within the specimen in addition to the external load record, allowing,e.g. to draw conclusions concerning the time of crack initiation. The shadow-optical method of caustics in reflection was applied for some of the specimens in order to determine the crack tip loading. The caustics were recorded with a 24-sparks high speed camera. In some cases the deformation pattern of the specimen surface was determined directly by high-speed photography of the specimen surface containing a scratched grid. Thus, the global bending displacement of the specimen and the opening of the crack flanks were determined.

The experiments were carried out at temperatures in the upper shelf of the Charpy energy (200 J) between room temperature and 90°C, most of them at 60°C. In all experiments the first phase of the crack propagation occured in a ductile mode. In all room temperature tests and even in some of the tests at 60°C the fracture mode changed into cleavage, in some cases followed by a second phase of ductile tearing. For the determination of the dynamic J-resistance curves only the first phase of ductile crack extension was evaluated. The resulting resistance curves are fairly independent of the test temperature.

Since for impact loading no standard evaluation scheme is available a procedure in accordance with ASTM E 813 and ASTM E 1152 (multi specimen technique) was chosen. Here, the J integral values are determined from the load displacement record P(s) and correlated with the corresponding ductile crack propagation Δa which was determined after the test by optical inspection of the fracture surfaces.

Fig. 3 shows dynamic J values versus the corresponding ductile crack extension for the SENB and Charpy specimens. Although not shown in the figure, the linear shape of the J-R curve for the SENB specimens above $\Delta a \sim 3$ mm is confirmed through further data points up to $\Delta a \sim 16$ mm. The J-R curve for the Charpy specimens results from 10 data points with only little scatter (see [1,2]).

The Charpy tests deliver J-values up to about 1 MN/m, while the results from the SENB specimens are significantly higher. Practically all J-values exceed the maximum J capacity J_{max} of the specimens as proposed in the standard (Charpy: J_{max} = 0,35 MN/m, SENB: J_{max} = 1,58 MN/m).

At a first glance the SENB data seem to follow the blunting line although the stretched zone width is only about 0,1 mm, indicating a significant amount of ductile crack

propagation for all data points reported. Only at very high J values of about 3,3 MN/m the initially very steep slope of the curve drops remarkably.

For comparison, Fig. 3 shows further results [4] from static tests with SENB specimens and with CT-25 specimens of the same heat. Two results from static SENB tests define a slope which nicely matches the slope of the dynamic curve for the SENB specimens for large amounts of crack extension. However, the absolute values of the static curve lie significantly below those from the dynamic curve. The static J-R curve from the compact specimens CT-25 forms the lower bound to all other curves.

2.2 Numerical simulations

In order to support the experimental results, especially concerning the evaluation of the J-integral, numerical simulations by the finite element method were performed [5]. In order to cover strain rate effects an elastic-viscoplastic material model was employed in the two-dimensional models. The J-integral was computed with a virtual crack extension method taking into account acceleration terms, and crack propagation was simulated by a node-release technique.

Modelling of the impact experiments turned out to be extremely complicated for two reasons. At a first glance it would be feasible to impose the measured reaction forces of the hammer on the specimen in order to model the dynamic loading event. However, the calculated displacements at a given force are very sensitive to details of the model and of the material law. Therefore, it was necessary to include the hammer as a point mass which comes into contact with the specimen surface through a spring representing the stiffness between the centre of gravity of the hammer and the specimen.

A second complication comes from the fact that during the test the specimens glide over the supports rather than having one fixed point of contact. This gliding is indicated by significant visible plastic deformations of the specimen and it is doubtful that the resulting friction force can be described by a Coulomb law.

Therefore, in [5] the numerical models had to be successively improved and checked against experimental observations. In the final model, the calculated hammer force as a function of time agrees very well with the measured one, Fig. 4. Despite the fact that the calculated J-integral values in Fig. 5 suffer from a certain path-dependency which could not be eliminated completely by the correction term the numerical simulation supports the rather high level of J-values in the experimental evaluation.

In order to increase the accuracy of future numerical simulations dynamic stress-strain curves must be available. Standard round bar tension specimens were tested in a gas gun device at impact velocities of about 20m/s. The load was measured by pairs of strain gauges attached to the ends of the specimens. The time-dependent local deformation and strain pattern was determined by high-speed photography (24-spark camera) of the specimen carrying a row of pins. Fig. 6 shows the loading arrangement and the specimen. A dynamic stress-strain curve at room temperature for an impact velocity of about 20 m/s is shown in Fig. 7. This curve lies significantly above the corresponding static curve.

2.3 Fractographic examinations

The most remarkable feature of the dynamic J-resistance curve obtained from the large SENB-specimens is the sudden change in slope at a J-level of about 3,3 MN/m corresponding to a crack extension of about 3 mm. However, the examination of the fracture surfaces by scanning electron microscopy revealed no indications of a change in fracture mode after a crack extension of about 3 mm. Therefore, additional metallographic sectionings perpendicular to the crack front were performed in order to reveal more details of the ductile failure process [1,2].

With the first specimen examined the section revealed a 3 mm long side crack next to the main crack, see Fig. 8. This length coincides with the amount of crack extension where the slope of the resistance curve changes. If it is assumed that higher energy increments per unit advance of the main crack are needed in the first phase of ductile

crack extension when more than one crack propagates at the same time than in the second phase with just one main crack the different slopes in the overall resistance curve is easily explained.

In contrast to the main crack showing the typical rough ductile surface the side crack appears rather smooth, indicating a shear mode of rupture. This is confirmed by microscopic inspection of the fracture surfaces, Fig. 9. Systematic examination of several specimens reveals that depending on the through-the-thickness position two- or even three-crack systems just in front of the original fatigue crack were found almost everywhere along the crack front. After a certain amount of crack extension only one of these competing cracks continues to grow. The fact that close to the notches of the side-grooves only the main crack is observed might be an indication, that the local triaxiality of the stress state ahead of the crack front (constraint) is of influence on the development of side cracks. Although a complete explanation of this mechanism is not yet possible the principal influence of loading rate and specimen size on this effect may be deduced at least qualitatively in Fig. 10.

Of particular interest for the evaluation of components is the fact that with increasing specimen size and loading rate the tendency to develop side cracks increases. This may lead to a significant elevation of the resistance curve. If the trends reported here could be confirmed additional safety margins could be expected for large reactor components in particular under sudden load changes.

3. CRACK PROPAGATION ENERGY R

Besides other limitations the standards require that the allowable crack propagation does not exceed one tenth of the ligament length of the specimen when a J-resistance curve is measured. Taking into account, e.g., C25-specimens this leads to a largest possible crack propagation of less than 3 mm. On the other hand, the realistic evaluation of worst-case plant situations often imply large amounts of ductile crack propagation far beyond these limits.

Therefore, it is necessary to extent the J-integral concept (see 3.1) or to introduce new concepts describing the propagation of cracks (see 3.2). One of these new concepts is the crack propagation energy which was introduced in [6] in analogy to the elastic energy release rate as the dissipated plastic fracture energy per newly formed crack surface. To check the applicability to reactor components and to establish correlations with the J-integral concept wide plates of ASTM A 508 Cl 2 (22 NiMoCr 3 7) were tested and evaluated. Fig. 11 shows schematically the specimen geometry and a typical instrumentation.

3.1 Static test

The test plate with dimensions 680 × 250 ×20 mm^3 was provided with a pre-fatigued edge crack with initial length of 125 mm and with 20% side-grooves. The load was applied through bolts supported by special elements designed to allow friction-free rolling of the bolts. In addition to load and bolt-displacement the crack-mouth-opening displacement (clip-gauges and scratched grid) and the strains at three positions on the plate were measured.

The partial unloading compliance method, the alternating current potential drop method, and direct optical observation were employed to determine the crack propagation. The J-integral was estimated from the area under the measured load vs. load line displacement record. Fig. 12 shows the resulting J-resistance curve together with the result of a finite element simulation. Because significant necking of the ligament was observed in the experiment a plane stress model was considered appropriate. The results of the simulation are in good agreement with the experimental curve.

3.2 Rapid loading

Three further plates of the same basic dimensions were tested with a load-point displacement-rate of 10 mm/s correponding to the maximum loading velocity of the machine. These loading conditions may still be considered quasi-static, but fast enough to ensure adiabatic conditions for heat transfer. In these tests the crack propagation was observed optically with a camera (37 frames/s). The evaluation of the pictures was assisted by an image processing system. In order to determine the crack propagation energy R it was assumed that practically all fracture energy is dissipated in the form of plastic work which results in a temperature rise in the plastically deformed areas. In every test the development of the temperature fields around the crack path were measured with thermocouples. In addition, the complete temperature field on the specimen surface was recorded by an infrared camera at a framing rate of 0,6 s. To this end the plane surfaces were coated with a thin oil film.

Fig. 13 shows the force F on the specimen and the mechanical energy U as a function of time. In Fig. 14 a bi-modal approximation of the derivative of U with respect to crack length a, dU/da, is plotted versus the relative position of the crack at the respective time. However, this is not the desired crack propagation energy R, because R includes plastic work and also plastic damage dissipated at times before the crack tip reaches a given position. Therefore, this value of about 1,4 MJ/m^2 for most of the curve, reflects only one specific time and is a lower bound to R for steady state crack propagation.

Consequently, the evaluation of the crack propagation energy R is done from the thermal measurements. Here, the temperature fields along lines perpendicular to the crack path are evaluated at different times with respect to plastic work dissipation expressed by the generated heat. These data points in terms of R are also plotted in Fig. 14. A fairly constant R of about 3,5 MJ/m^2 is found throughout the whole crack propagation distance. This value agrees very well with the average R obtained if the total mechanical energy is divided by the total crack area generated during the test. This confirms the assumption that the R is identical with the dissipated energy transformed almost completely into heat.

ACKNOWLEDGEMENT:

The authors are grateful to the German Minister of Research and Development (BMFT) who sponsored part of this work.

REFERENCES:

[1] Böhme, W. (1989), Experimentelle Untersuchungen zum elastisch-plastischen Bruchver halten eines Druckbehälterstahls unter dynamischer Beanspruchung, IWM-Bericht W 3/89, Fraunhofer-Institut für Werkstoffmechanik, Freiburg

[2] Böhme, W. and Schmitt, W. (1991), On the Ductile Crack Initiation and Propagation Behavior of a Pressure Vessel Steel Under Impact Loading, in: Defect Assessment in Components - Fundamentals and Applications, Eds.: J.G. Blauel and K.-H. Schwalbe, Mech. Eng. Publ. London (MEPL)

[3] Böhme, W. (1990), On the Fracture Resistance of a Pressure Vessel Steel under Impact Loading Conditions, ASTM Symposium on Rapid Load Fracture Testing, San Francisco, to be published in ASTM STP

[4] Blauel, J.G., Böhme, W., Schäfer, R., Voss, B. and Winkler, S. (1990), Bruchmecha nik-Experimente und numerische Analysen zur Zähbruchinitiierung, IWM-Bericht Z 10/90, Freiburg

[5] Vo, T. and Stöckl, H. (1989), Simulation von Schlagversuchen an großen Biegeproben aus einem Druckbehälterstahl mit der Methode der Finiten Elemente, IWM-Bericht W 2/89, Freiburg

[6] Klemm, W. (1989), Material Resistance Against Fast Ductile Fracture in Pipeline Steels, Dyn. Fract. Mech. for the 1990's, ASME-JSME Pressure Vessels and Piping Conference, Honolulu, Hawaii, Eds. H. Homma, D.A. Shockey, G. Yagawa

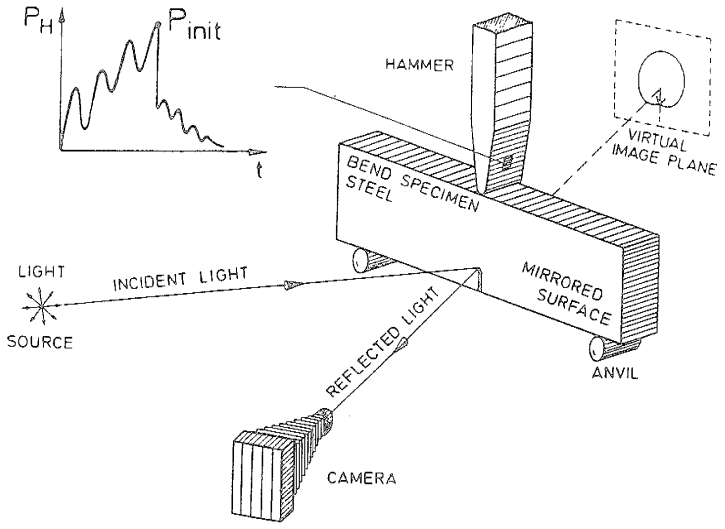

Fig. 1 Experimental set-up for impact tests

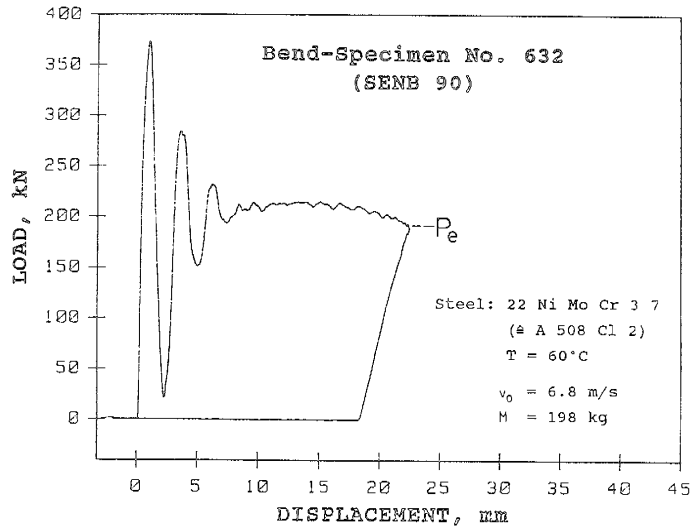

Fig. 2: Load-displacement record for drop-weight loaded SENB-specimen

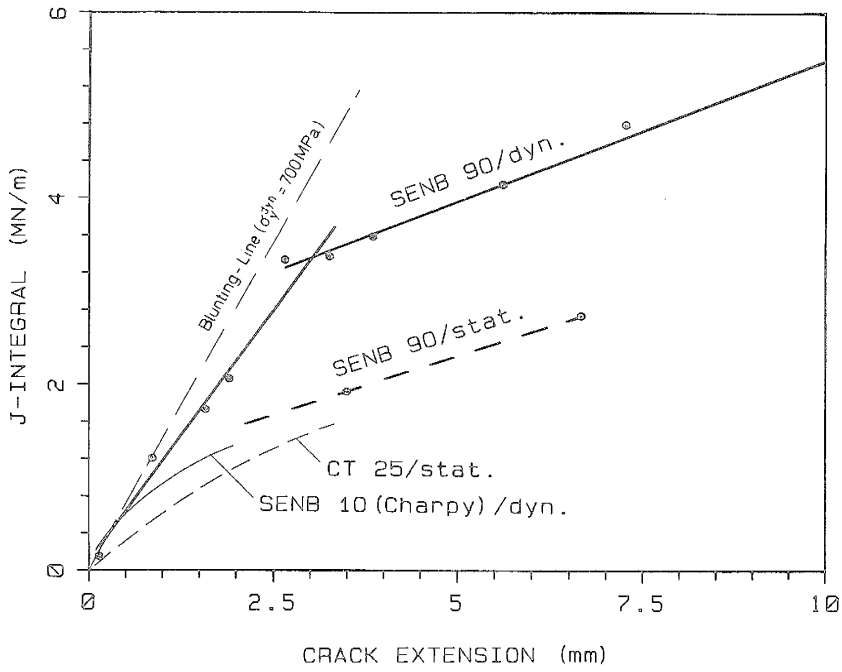

Fig. 3: Dynamic and static J-resistance curves

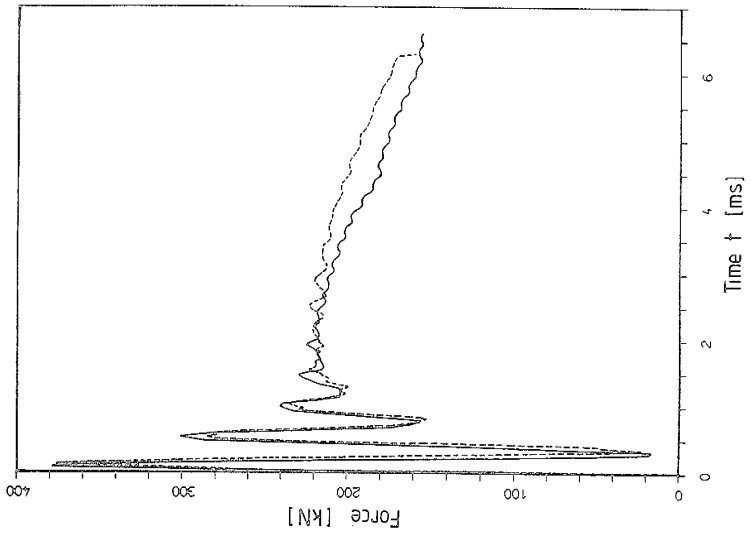

Fig. 4: Calculated and measured hammer forces for SENB-specimen

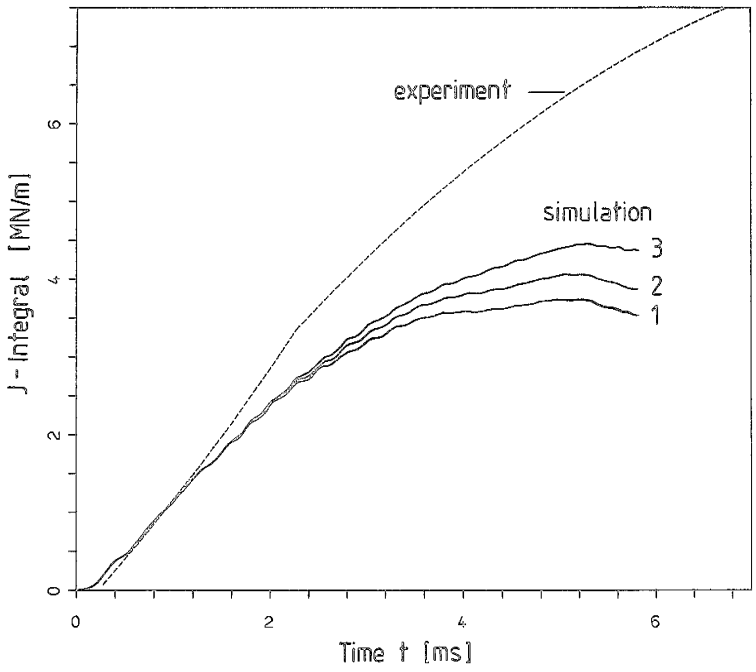

Fig. 5: Experimental and calculated J integral vs. time

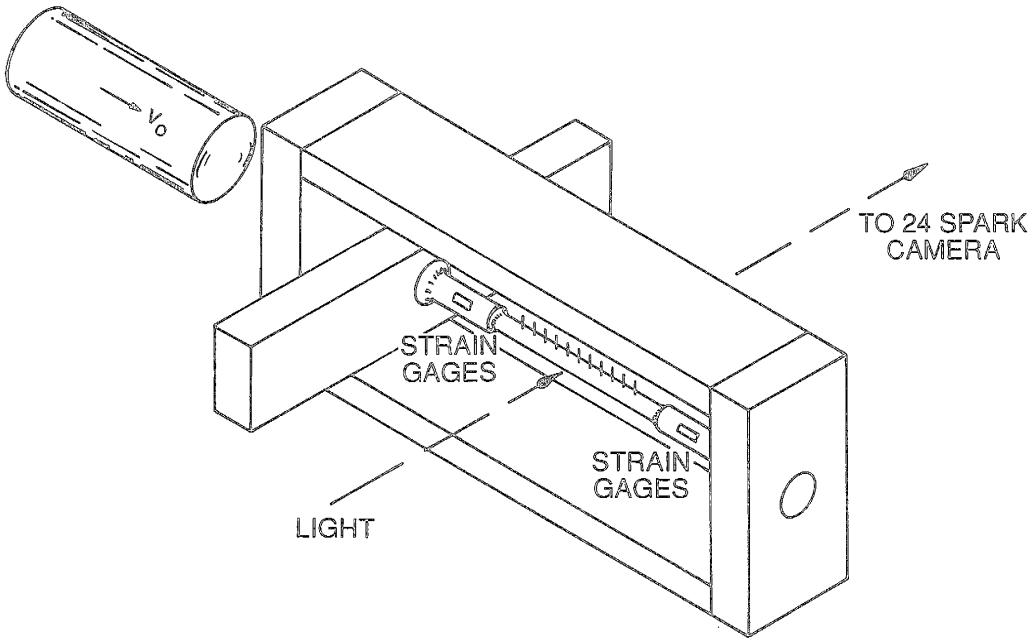

Fig. 6: Loading arrangement for dynamic tension tests

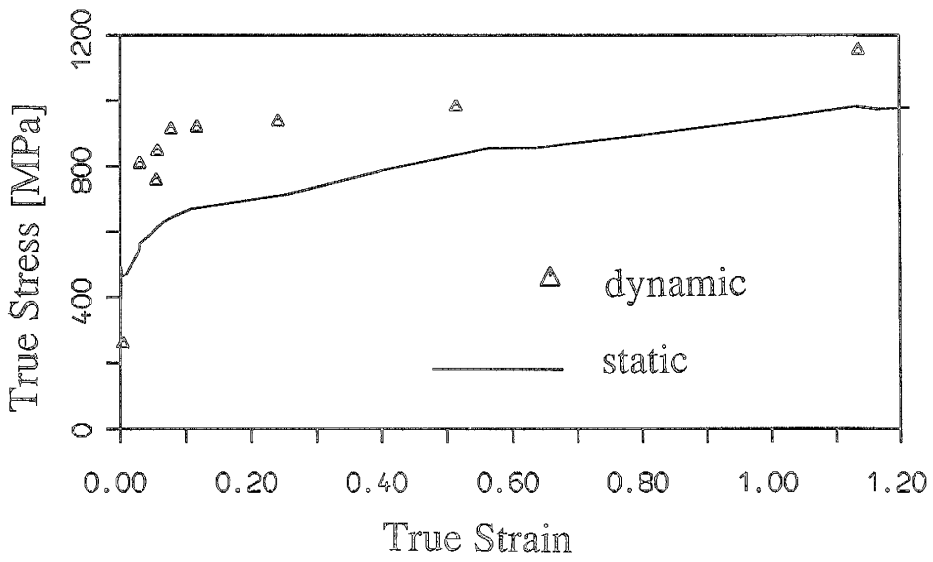

Fig. 7: Dynamic and static stress-strain curves

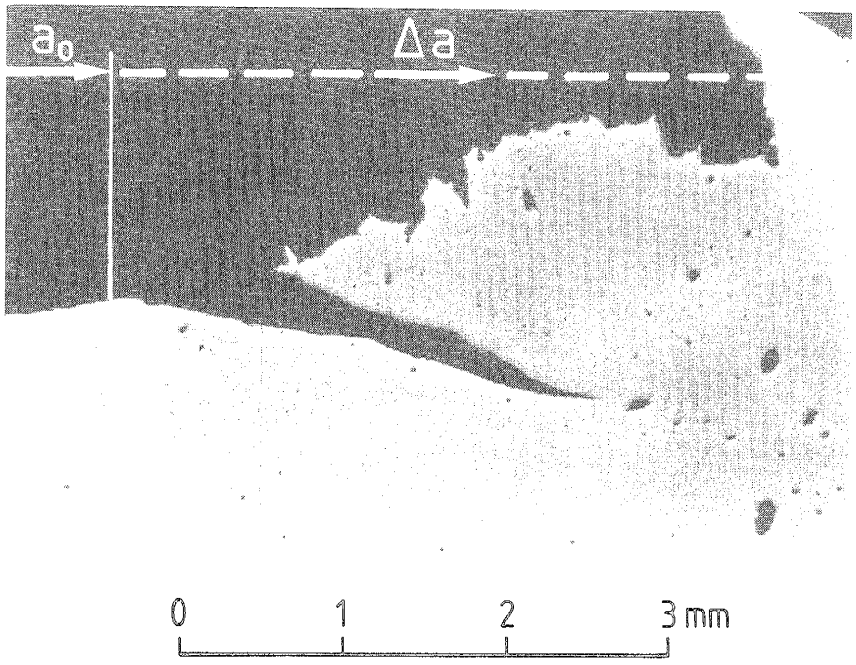

Fig. 8: Metallographic sectioning of SENB-specimen with side crack

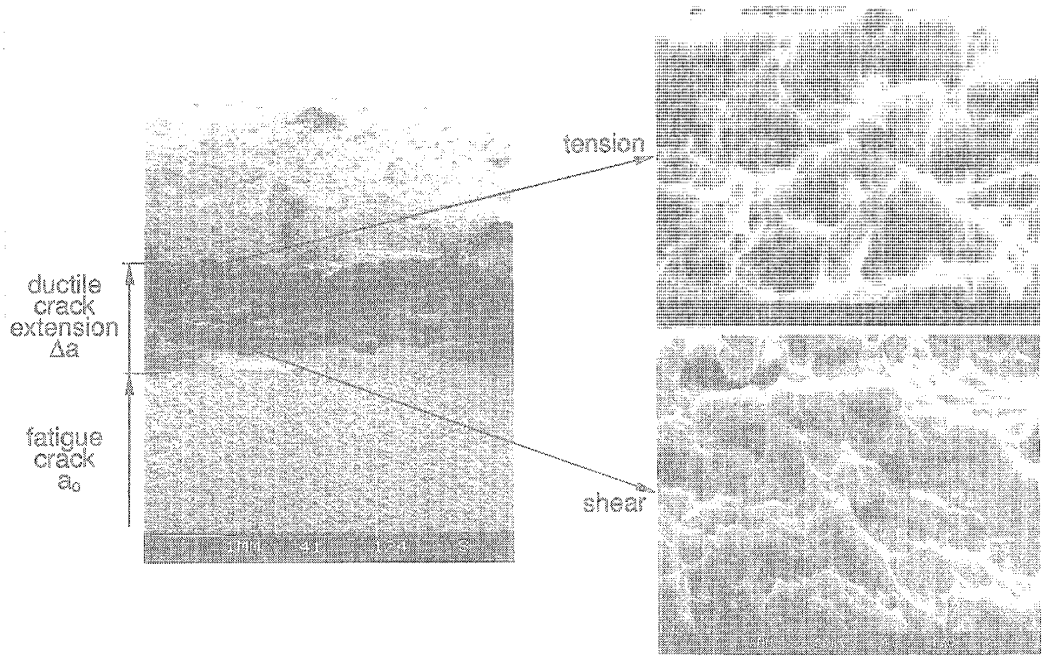

Fig. 9: Microscopic fracture appearance of side crack and main crack

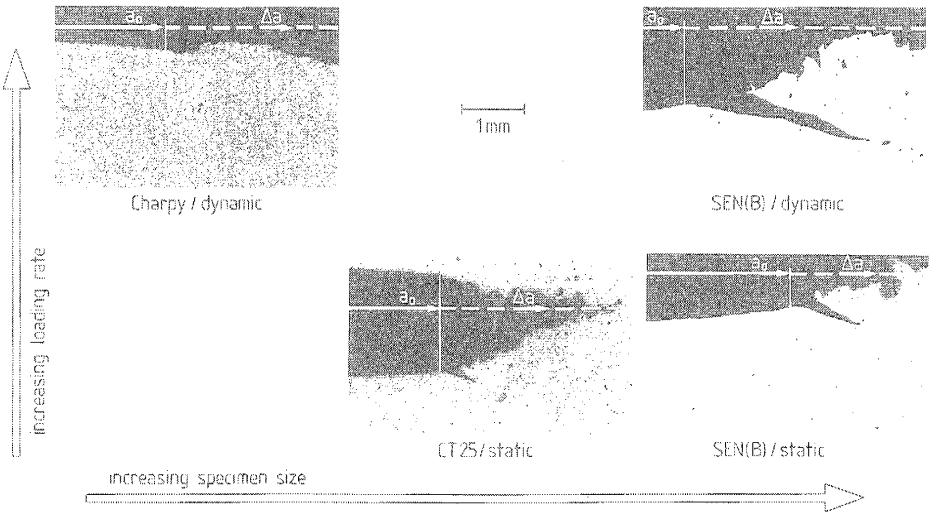

Fig. 10: Effect of loading rate and specimen size on side crack development

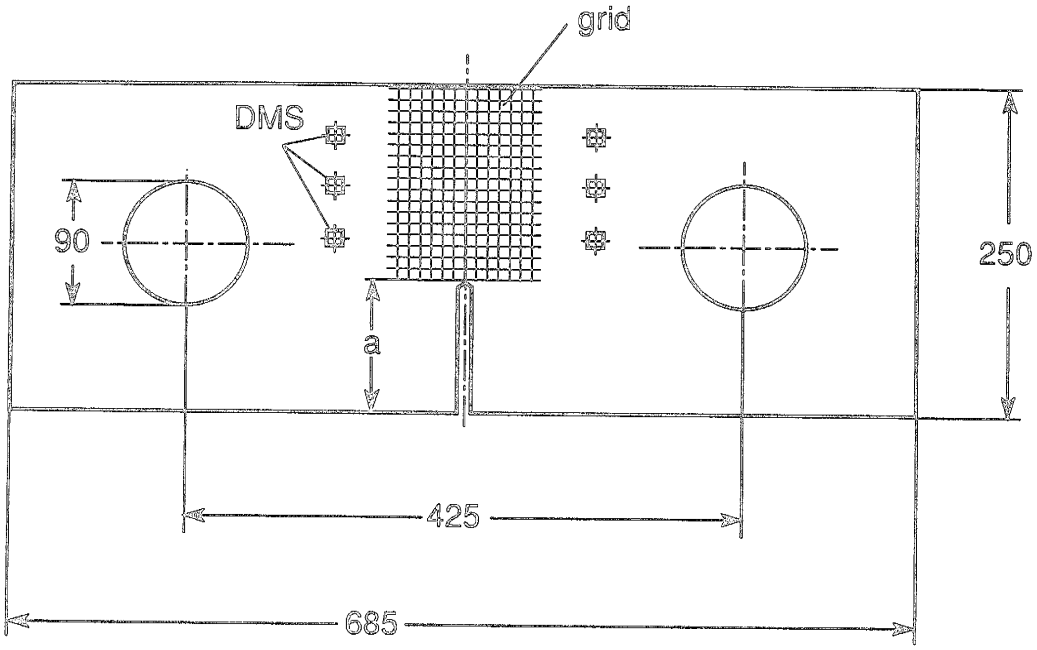

Fig. 11: Wide plate specimen with instrumentation

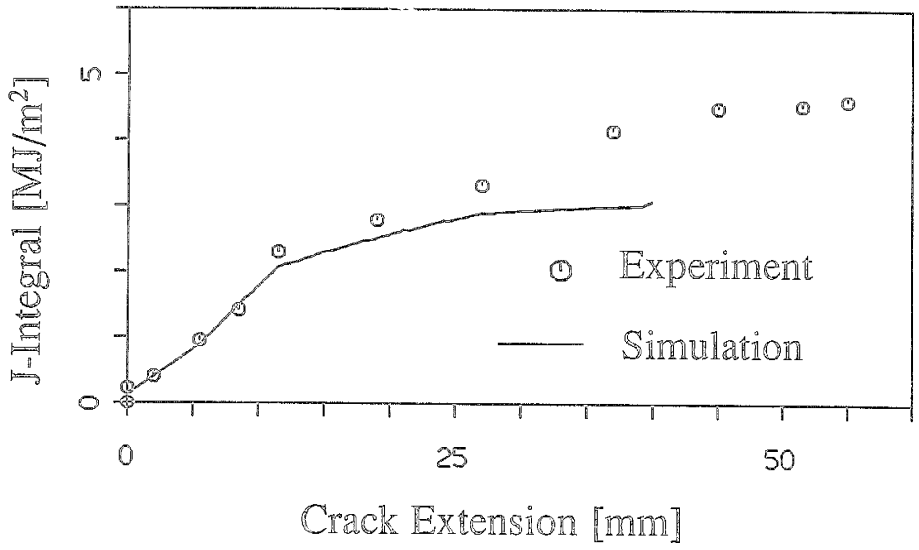

Fig. 12: Experimental and calculated J-R curves for wide plate test

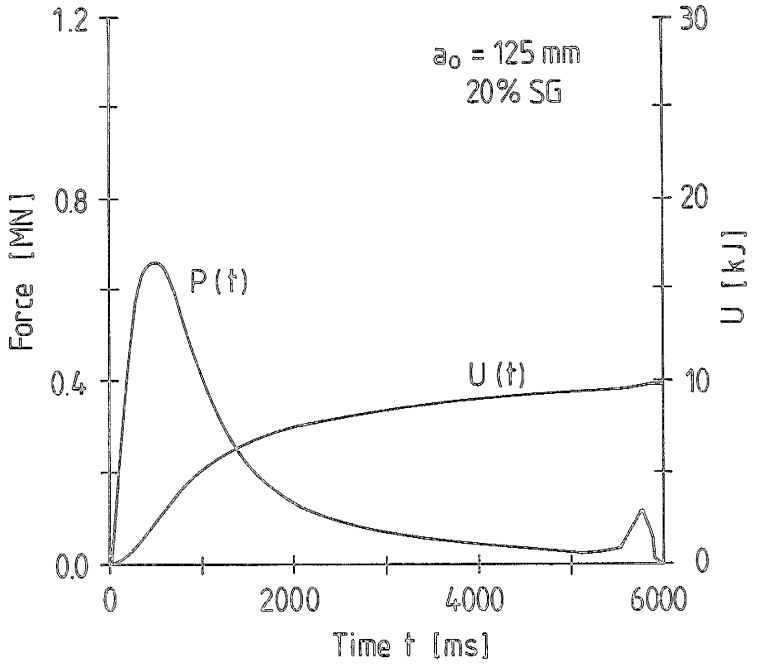

Fig. 13: Force and mechanical energy vs. time

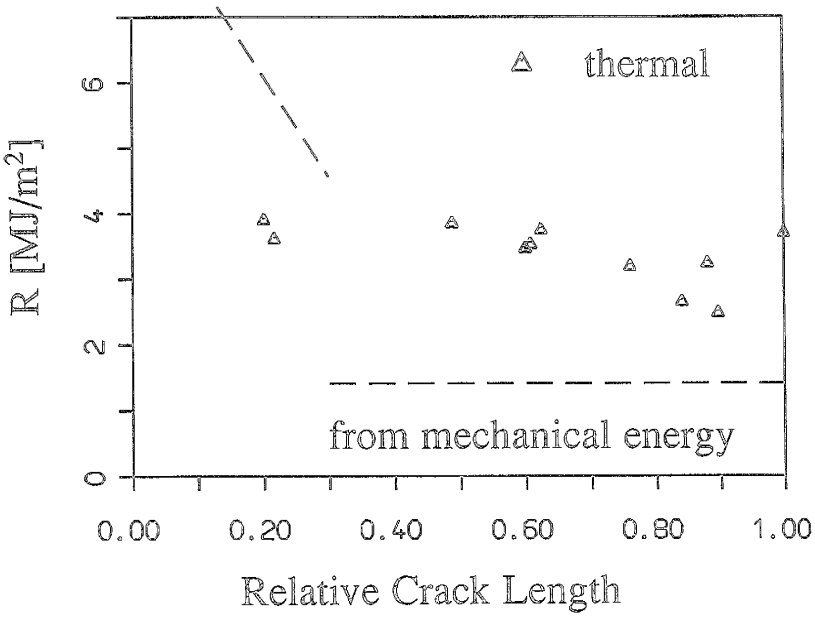

Fig. 14: Crack propagation energy R